Efficient Plasma Route to Nanostructure Materials: Case Study on the Use of m-WO₃ for Solar Water Splitting

Moreno de Respinis,*,[†] Gregory De Temmerman,[‡] Irem Tanyeli,[‡] Mauritius C.M. van de Sanden,[‡] Russ P. Doerner,[§] Matthew J. Baldwin,[§] and Roel van de Krol[†,‖]

[†]Faculty of Applied Sciences, Department of Chemical Engineering, Materials for Energy Conversion and Storage, Delft University of Technology, P.O. Box 5045, 2600 GA Delft, The Netherlands

[‡]FOM-Institute DIFFER, Dutch Institute For Fundamental Energy Research, P. O. Box 1207, 3430 BE Nieuwegein, The Netherlands

[§]Center for Energy Research, University of California at San Diego, 9500 Gilman Drive, La Jolla, California, United States

[‖]Institute for Solar Fuels, Helmholtz-Zentrum Berlin für Materialien und Energie Gmbh, Hahn-Meitner-Platz 1, 14109 Berlin, Germany

ⓢ *Supporting Information*

ABSTRACT: One of the main challenges in developing highly efficient nanostructured photoelectrodes is to achieve good control over the desired morphology and good electrical conductivity. We present an efficient plasma-processing technique to form porous structures in tungsten substrates. After an optimized two-step annealing procedure, the mesoporous tungsten transforms into photoactive monoclinic WO₃. The excellent control over the feature size and good contact between the crystallites obtained with the plasma technique offers an exciting new synthesis route for nanostructured materials for use in processes such as solar water splitting.
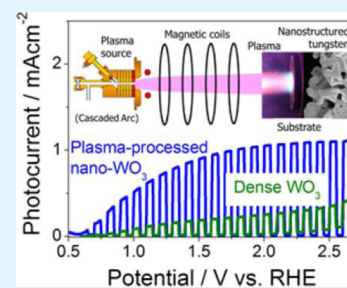
■ INTRODUCTION

One of the grand challenges for the 21st century is to secure the availability of energy on demand on the terawatt scale.[1] Moreover, environmental concerns result in the need for renewable energy sources to satisfy this demand. The direct photoelectrochemical conversion of solar energy into storable fuels, which is based on cheap and earth-abundant semiconductors and catalysts, has the potential to satisfy these requirements. Metal-oxide semiconductors are particularly appealing candidates for practical applications because of their low cost, nontoxicity, abundance, and stability toward corrosion.[2]

Despite intensive research efforts over the past 40 years, the efficiency of direct solar water splitting using metal oxides processed via scalable techniques still remains low.[3,4] One of the main bottlenecks for achieving high efficiencies with metal oxides is the mismatch between the absorption depth of visible light (up to micrometers) and the distance that the photogenerated charge carriers can travel before they recombine. The latter is often one order of magnitude shorter than the penetration depth of the light. A second limiting factor is the slow reaction kinetics at the surface of most metal oxides, especially for water oxidation.

Morphology control can overcome these challenges. Specifically, geometries with a large surface-to-volume ratio, such as nanowire arrays and porous nanostructures, will decrease the distance over which charge transport has to occur and increase the amount of available surface area for catalytic reactions.[5−7] Although a great variety of techniques are available nowadays to fabricate nanostructured materials, it is often difficult to achieve the desired combination of properties. For example, standard approaches such as wet-chemical processing can give very homogeneous particle sizes, but the contact between the particles is often poor and a necking treatment is needed to alleviate this limitation.[8]

In this Article, we propose a novel processing technique based on the surface treatment of tungsten substrates by a high flux of low-energy helium ions. This provides an efficient route for the formation of porous metallic nanostructures that, after oxidation, can be used as photoanodes for solar water splitting. The exposure of metal surfaces at elevated temperatures to high fluxes of low-energy (<100 eV) helium ions has been shown to lead to the formation of a nanostructured surface morphology consisting of nanometric filaments.[9] The structure size can be controlled by the processing temperature, whereas the thickness of the nanostructured layer depends on the processing time.[10] The porosity of the processed material is very high (up to 90%), and this yields a very high light absorption (up to 99%) across the whole visible spectrum.[11] Moreover, the continuous structure ensures that efficient
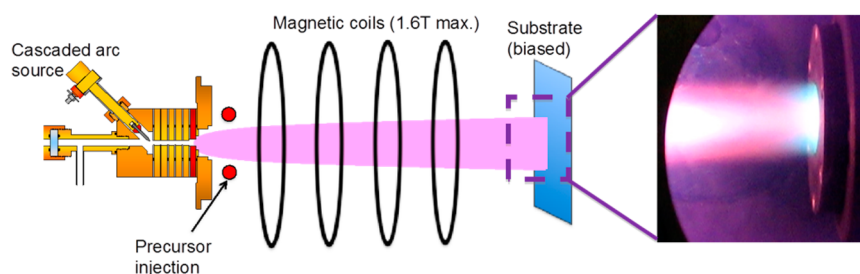
Figure 1. Schematic overview of the high-flux plasma generator used to generate the helium-induced nanostructured surfaces. The plasma is generated by a cascaded arc discharge and confined by a strong magnetic field. The picture on the right shows the high-intensity helium beam interacting with a tungsten surface.

charge transport through the structure is possible without the need for postdeposition necking treatments.

Tungsten is chosen for this case-study because of the high photocatalytic activity of its oxide, WO_3, in the monoclinic phase. Nanostructuring is essential for this material to address the mismatch between the intrinsically low light absorption coefficient ($1/_\alpha$ = 6 μm at λ = 327 nm^{12}) and the modest minority (hole) carrier diffusion length ($\sim$150 nm[12]). Previous studies have shown that nanoporosity indeed improves the incident photon-to-current efficiency (IPCE) of WO_3 photoanodes.[13] Santato et al. have reported on mesoporous nanocrystalline WO_3 photoanodes that showed an IPCE as high as 97% under UV illumination (380 nm) in the presence of a sacrificial hole scavenger (MeOH).[14−16] Berger et al. have shown that randomly oriented porous layers of WO_3 generate significantly higher photocurrents than compact layers resulting from different mechanisms of charge separation.[17] Tungsten oxide photoelectrodes for photoelectrochemical water splitting are mostly synthesized via sol−gel methods[14−16,18] or hydrothermal synthesis followed by calcination[19,20] and to lesser extent via CVD, pulsed electrodeposition, and reactive sputtering.[21,22] With most of these techniques, stoichiometric WO_3 is obtained during the synthesis process, and a standard thermal annealing is required to form the desired highly crystalline monoclinic phase. Other studies have been published on the formation of dense tungsten oxide films directly from tungsten metal by thermal treatment at elevated temperatures.[23−26] However, poor control over the stoichiometry[24] and thickness of the oxide layer[25,26] has prevented any efficient application of these methods for solar water splitting. In this Article, we will show how the novel plasma-treatment technique can overcome these issues.

EXPERIMENTAL SECTION

Polycrystalline tungsten discs (25 mm in diameter and 1 mm in thickness) were cut from a rod of rolled tungsten (Plansee, 99.95 wt % purity) and mechanically polished to a mirror finish. After polishing, they were rinsed in alcohol and acetone and no further treatment was applied. Surface nanostructuring was performed using high fluxes of low-energy helium ions in a plasma generator (Figure 1). It has been previously demonstrated that helium-induced nanostructure formation on tungsten surfaces worked best when the particle flux to the surface is higher than 7×10^{21} m^{-2} s^{-1}. The helium plasma is generated by a magnetically confined arc discharge.[27] The nanorod dimensions (length and diameter) depend on the processing time and temperature, respectively. For this case study, nanorod diameters in the range 100−200 nm were chosen. The nanostructure was formed by exposing the tungsten surface to 150 eV helium ions with a flux of 8×10^{23} m^{-2} s^{-1} at a surface temperature of 1700 K (1427 °C) for a duration of 1000 s.

Nanostructured tungsten targets are annealed either with a single-step treatment at 550 °C for 8 h following a modified procedure from the literature[15] or via an optimized two-step thermal oxidative annealing to form WO_3. The procedure consists of a short thermal treatment of 2 h at 550 °C followed by further annealing at 450 °C for 4 h (all in flowing O_2). Polished samples are annealed either under the same two-step procedure or with a single-step treatment at 700 °C for 60 min following a modified procedure from the literature.[23,26]

The crystal structure of the samples was determined using a Bruker D8 Advance X-ray diffractometer equipped with LynxEye linear detector in a Bragg−Brentano configuration. A PerkinElmer Lambda 900 UV/vis/NIR double-beam spectrophotometer with an integrating sphere was used for diffuse reflectance measurements.

Photoelectrochemical characterization was carried out in an aqueous 3 M H_2SO_4 (95−97%, Sigma-Aldrich) solution. The faradaic efficiency of WO_3 in different electrolytes has recently been examined, and it is noted that in H_2SO_4 WO_3 may produce persulfate more favorably than O_2.[40] However, this is not expected to change the photocurrent, and the application of the right cocatalyst probably overcomes this issue. The solution was purged with nitrogen prior to and during the measurements to remove any dissolved oxygen. Potential control was provided by a potentiostat (EG&G PAR 283) in a three-electrode cell with a fused silica window.[2] An Ag/AgCl electrode (XR300, Radiometer Analytical) and a coiled Pt wire were used as the reference and counter electrodes, respectively. White-light photocurrent densities were measured under simulated AM1.5 solar illumination (100 mW/cm^2) with a Newport Sol3A Class AAA solar simulator (type 94023A-SR3), whereas quantum efficiencies were measured with a 300 W Xe-arc lamp (L.O.T. Oriel LSB530U) coupled into a grating monochromator (Acton SpectraPro 150i). An electronic shutter (Uniblitz LS6) and high-pass colored glass filters (Schott, two filters of 3 mm thickness each) were placed between the monochromator and the sample to remove second-order diffracted light. The intensity of the monochromatic light was measured with a calibrated photodiode (Ophir PD300-UV).

RESULTS AND DISCUSSION

After treatment with low-energy helium ions, the tungsten surfaces exhibit a nanostructured surface morphology consisting of nanometric filaments with an open interconnected structure. Figure 2b illustrates the typical morphology observed for a surface temperature of 1500 °C. The formation mechanism of such structures has been studied in detail and appears to be linked to the formation and coalescence of helium bubbles in the near-surface region, inducing swelling of the surface.[15] At 1500 °C, the nanoscopic filaments have a diameter of 100−200 nm (Figure 2a,b). We recently showed that these filaments have a crystalline inner structure.[10] The formation of such nanostructures occurs when the particle flux to the surface during processing is sufficiently high[28] (i.e., when the helium concentration in the near-surface region during the plasma processing is high enough for helium bubbles to grow and
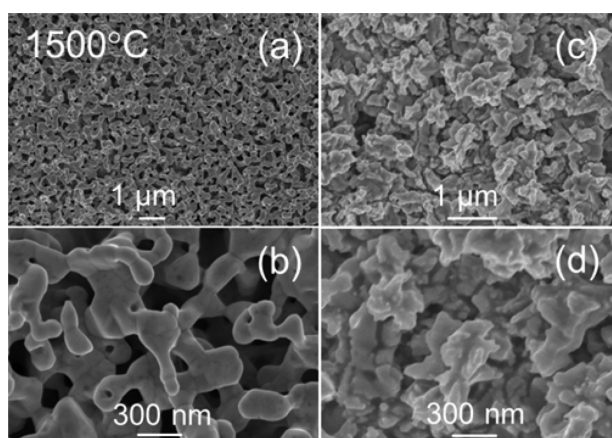
Figure 2. (a, b) SEM images of plasma-processed tungsten metal at two different magnifications. (c,d) Resulting WO$_3$ samples after the two-step annealing.

coalesce). With a porosity of up to 90%, the nanostructured tungsten absorbs between 94 and 97% of light in the visible range, whereas the polished targets reflect more than 50% of the light (Figures 3a,d and 4a). Although a detailed quantitative
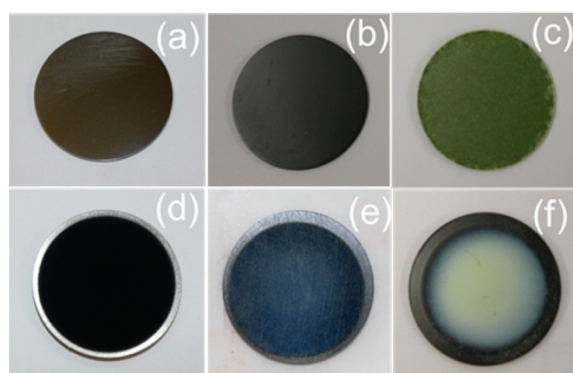

Figure 3. Photographs of (a) polished tungsten, (b) polished tungsten after two-step annealing at 550 and 450 °C, (c) polished tungsten after annealing at 700 °C, (d) nanostructured tungsten, (e) nanostructured tungsten single-step annealed at 550 °C, and (f) nanostructured tungsten after two-step annealing at 550 and 450 °C.
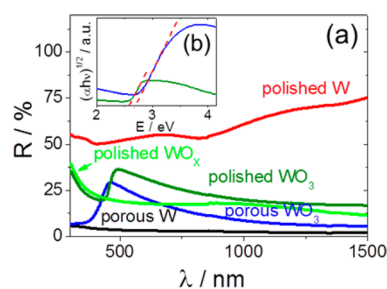

Figure 4. (a) Diffuse reflectance measurements of polished tungsten (red), polished tungsten after two-step annealing (green), nanostructured tungsten (black), nanostructured WO$_3$ after two-step annealing (blue), and polished tungsten after annealing at 700 °C (olive). (b) Kubelka−Munk transformation of the reflectance curves for nanostructured WO$_3$ after two-step annealing (blue) and for polished W after annealing at 700 °C (polished WO$_3$) (olive).

analysis of the porosity and specific surface area is beyond the scope of this study, nonoxidized metallic W films made with the

same plasma technique by Kajita et al. indeed showed porosities of up to 90% at the surface and about 50% near the bottom of the nanostructure.[41] The specific surface area of these metallic W films, as measured by nitrogen adsorption (BET), can be ~20 times higher than the geometrical area.[42]

After the plasma processing, the tungsten samples were annealed under a flow of oxygen in either one or two steps. The first step is carried out at 550 °C for 2 h to obtain the desired monoclinic WO$_3$ (m-WO$_3$) phase.[16] Although high temperatures favor fast crystallization, they also present more strongly reducing conditions. To avoid the possibility that this leads to the formation of a substoichiometric WO$_{3-x}$ phase, the sample was subsequently held at a somewhat lower temperature (450 °C) for 4 h to oxidize fully the sample before cooling to room temperature. This temperature allows for the full oxidation of the mesoporous structure and prevents extensive oxidation of the dense tungsten substrate underneath.

The effect of the two-step treatment can be seen by comparing panels e and f in Figure 3. Samples annealed with a single step at 550 °C have a blue color (Figure 3e), indicating the presence of oxygen vacancies. The same blue color was also observed for annealing temperatures of 500 and 600 °C and for a prolonged 8 h treatment at 550 °C (not shown). The blue coloration of the oxygen-deficient WO$_{3-x}$ phase is well known and extensively documented in the literature.[26,29−34,43] After the second annealing for 4 h at 450 °C, the sample turns yellow (Figure 3f). This corresponds to the color of stoichiometric WO$_3$, indicating that the sample indeed fully oxidizes at this lower temperature.

A more detailed analysis of the optical properties is shown in Figure 4. After the two-step annealing, the porous WO$_3$ samples show a sharp decrease of the diffuse reflectance below ~470 nm that marks the optical absorption edge (band gap) of the material (Figure 4a). In contrast, polished samples annealed under the same two-step procedure do not show such a transition. This suggests that the oxidation of the surface of bulk tungsten is much slower than that of the porous nanostructured material. Firing the polished sample at a much higher temperature (700 °C) leads to a greenish coloration of the sample (Figure 3c) and a sharp decrease in the reflectance below ~480 nm (Figure 4a) that is consistent with the presence of m-WO$_3$. X-ray diffraction indeed confirms the formation of a monoclinic WO$_3$ phase under these conditions (Figure S1, Supporting Information). The fact that this sample is greenish (i.e., a mixture of yellow and blue) suggests the presence of a significant amount of substoichiometric WO$_{3-x}$.

The Kubelka−Munk transformation[35,36] of the diffuse reflectance curves, shown in Figure 4b, shows band-gap values of 2.7 and 2.6 eV for the porous and polished m-WO$_3$ samples, respectively. In the literature, the band-gap energy of WO$_3$ has been mainly measured by optical absorption, varying from about 2.5 to 3.0 eV.[37,38] According to Berger et al., the band gap of porous structures is the same as that for compact ones;[17] therefore, the different morphology cannot explain the different band gaps in Figure 4b. Instead, we attribute the difference to the different annealing conditions. This is consistent with literature reports that show that the band gap of WO$_3$ undergoes a red shift upon annealing at higher temperatures.[19,20,39]

The photoelectrochemical activity of the WO$_3$ samples was determined by measuring the current as a function of the applied potential under chopped AM1.5 illumination (Figure
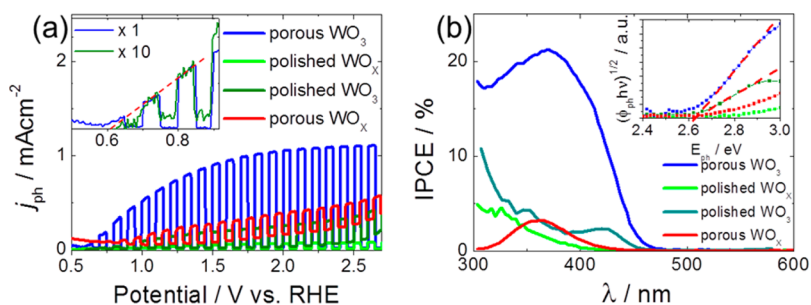
7623

dx.doi.org/10.1021/am401936q | ACS Appl. Mater. Interfaces 2013, 5, 7621−7625

Figure 5. (a) J-V curve under chopped AM1.5 illumination of polished tungsten after two-step annealing (polished WO_x, green), nanostructured WO_3 after two-step annealing (porous WO_3, blue), polished tungsten after annealing at 700 °C (polished WO_3, olive), and nanostructured WO_x annealed at 550 °C (porous WO_x, red). The scan rate was 10 mV/s. The inset shows a photocurrent onset potential of +0.6 V vs RHE for both the porous WO_3 and polished WO_3 (zoomed 10×). (b) IPCE measured at 1.23 V vs RHE and 2 nm/sec (inset shows the band gap).

5a). The porous nanostructured samples made with the plasma-processing method and annealed using the two-step procedure at 550 and 450 °C show a significantly higher photocurrent-plateau value than the polished sample annealed at 700 °C: 6 times higher at 1.0 V versus RHE and 3 times higher at 2.5 V versus RHE. The higher photocurrent of the nanostructured sample is attributed to three factors. The first is the higher specific surface area, which greatly enhances the catalytic activity for water oxidation. This is especially important at higher potentials where charge separation is efficient and the surface reaction kinetics struggle to keep up with the rapid supply of photogenerated holes. The second factor is the enhanced absorption resulting from extensive light scattering in the nanostructured material. This is also evident from the smaller reflectance (i.e., larger absorbance) of the nanoporous versus polished WO_3 in Figure 4a. The third factor is the fact that the typical feature size (Figure 2) is comparable to the minority carrier diffusion length (L_D ~150 nm[12]). This means that the photogenerated holes have no trouble reaching the semiconductor/electrolyte interface before they recombine. An important advantage of the plasma-processing technique is that the small feature size is retained even deep within the bulk of the porous film close to the interface with metallic tungsten (Figure S2, Supporting Information). This is especially important when considering the intrinsically low optical absorption coefficient of WO_3 ($1/\alpha$ = 6 μm at λ = 327 nm[12]).

The low photocurrent of the porous WO_x sample annealed in a single step at 550 °C (Figure 5a, red curve) is attributed to recombination at structural defects. These defects are presumably the oxygen vacancies that also cause the blue color of the material (Figure 3e).

A more detailed look at the voltammogram at low potentials reveals that the photocurrent of the nanostructured WO_3 increases more steeply than that of the compact WO_3. This is again a manifestation of the feature size being smaller than the minority carrier diffusion length. Within a distance L_D from the surface, all the holes can reach the electrolyte even without the presence of an electric field. Thus, at low applied potentials (close to V_{FB}), the porous sample will give higher currents because it has a larger surface area (i.e., there are more electron/hole pairs that are created within 150 nm of the surface than for the dense sample). At more positive potentials, the electric field can also separate the electron/hole pairs generated in the bulk of the material, resulting in the difference between the two morphologies becoming less important.

Both the polished and nanostructured WO_3 samples show an onset potential of 0.6 V versus RHE (inset of Figure 5a). This is

0.2 V more positive than the flat band potential of WO_3, which is +0.4 V versus RHE.[5] This difference is not unexpected for a metal oxide without a cocatalyst for O_2 evolution. In fact, for most (uncatalyzed) metal oxides, the difference between the flat band potential and the photocurrent onset potentials is much larger.

The AM1.5 photocurrent density of our compact WO_3 is similar to the values reported in the literature.[17,20,23,25] In contrast, the photocurrent densities for our plasma-treated nanostructured WO_3 are significantly higher than literature values for porous WO_3 synthesized directly from metallic W (although an accurate quantitative comparison cannot be made because of the different experimental conditions).[21] Quantum efficiency measurements (IPCE) in Figure 5b confirm the higher photoresponse over the whole spectrum of the above band-gap light for the porous WO_3. The efficiency peaks at 370 nm and reaches a value of 22%. The band gap of 2.65 eV obtained from the Tauc plot of the photocurrent (inset of Figure 5b) matches the value from the diffuse reflectance spectra (Figure 4b) and values reported in the literature for monoclinic WO_3.

■ CONCLUSIONS

In this Article, we have proposed a novel plasma-assisted processing technique to generate surface nanostructures on metals. This top-down approach guarantees good contact between the different crystallites and avoids electrical conductivity limitations. After an optimized two-step annealing procedure that minimizes the concentration of defects, the mesoporous metallic tungsten transforms into nanostructured monoclinic WO_3. These WO_3 films showed photocurrents of up to 1 mA/cm², which is 5 times higher than dense, nonporous WO_3 samples made from a polished W disc. The excellent control over the feature size with the helium-plasma technique along with its effectiveness with a broad range of metals offers an exciting new synthesis route for nanostructured materials for use in processes such as solar water splitting.

■ ASSOCIATED CONTENT

ⓢ Supporting Information

XRD patterns of the annealed samples and cross-section SEM image of a plasma-processed tungsten target. This material is available free of charge via the Internet at http://pubs.acs.org.

■ AUTHOR INFORMATION

Corresponding Author
*E-mail: M.deRespinis@TUDelft.nl.

Notes

The authors declare no competing financial interest.

REFERENCES

(1) Lewis, N. S.; Nocera, D. G. Proc. Natl. Acad. Sci. U.S.A. 2006, 103, 15729−15735.

(2) Photoelectrochemical Hydrogen Production Van de Krol, R., Grätzel, M., Eds.; Springer: New York, 2012.

(3) Chen, X.; Shen, S.; Guo, L.; Mao, S. S. Chem. Rev. 2010, 110, 6503−6570.

(4) Zou, Z.; Ye, J.; Sayama, K.; Arakawa, H. Nature 2001, 414, 625−627.

(5) Alexander, B. D.; Kulesza, P. J.; Rutkowska, I.; Solarska, R.; Augustynski, J. J. Mater. Chem. 2008, 18, 2298−2303.

(6) Van de Krol, R.; Liang, Y.; Schoonman, J. J. Mater. Chem. 2008, 18, 2311−2320.

(7) Thomann, I.; Pinaud, B. A.; Chen, Z.; Clemens, B. M.; Jaramillo, T. F.; Brongersma, M. L. Nano Lett. 2011, 11, 3440−3446.

(8) Abe, R.; Higashi, M.; Domen, K. J. Am. Chem. Soc. 2010, 132, 11828−11829.

(9) Baldwin, M. J.; Doerner, R. P. Nucl. Fusion 2008, 48, 035001-1−035001-6.

(10) De Temmerman, G.; Bystrov, K.; Zielinski, J. J.; Balden, M.; Matern, G.; Arnas, C.; Marot, L. J. Vac. Sci. Technol., A 2012, 30, 041306-1−041306-6.

(11) Kajita, S.; Saeki, T.; Yoshida, N.; Ohno, N.; Iwamae, A. Appl. Phys. Express 2010, 3, 085204-1−085204-3.

(12) Butler, M. A. J. Appl. Phys. 1977, 48, 1914−1920.

(13) Chen, X.; Ye, J.; Ouyang, S.; Kako, T.; Li, Z.; Zou, Z. ACS Nano 2011, 5, 4310−4318.

(14) Santato, C.; Ulmann, M.; Augustynski, J. J. Phys. Chem. B 2001, 105, 936−940.

(15) Santato, C.; Ulmann, M.; Augustynski, J. Adv. Mater. 2001, 13, 511−514.

(16) Santato, C.; Odziemkowski, M.; Ulmann, M.; Augustynski, J. J. Am. Chem. Soc. 2001, 123, 10639−10649.

(17) Berger, S.; Tsuchiya, H.; Ghicov, A.; Schmuki, P. Appl. Phys. Lett. 2006, 88, 203119−203122.

(18) Hsiao, P.-T.; Chen, L.-C.; Lia, T.-L.; Teng, H. J. Mater. Chem. 2011, 21, 19402−19409.

(19) Qin, D.-D.; Tao, C.-L.; Friesen, S. A.; Wang, T.-H.; Varghese, O. K.; Bao, N.-Z.; Yang, Z.-Y.; Mallouk, T. E.; Grimes, C. A. Chem. Commun. 2012, 48, 729−731.

(20) Hong, S. J.; Jun, H.; Borse, P. H.; Lee, J. S. Int. J. Hydrogen Energy 2009, 34, 3234−3242.

(21) Baeck, S. H.; Jaramillo, T.; Stucky, G. D.; McFarland, E. W. Nano Lett. 2002, 2, 831−834.

(22) Vemuri, R. S.; Engelhard, M. H.; Ramana, C. V. ACS Appl. Mater. Interfaces 2012, 4, 1371−1377.

(23) Gissler, W.; Memming, R. J. Electrochem. Soc. 1977, 124, 1710−1714.

(24) Gu, G.; Zheng, B.; Han, W. Q.; Roth, S.; Liu, J. Nano Lett. 2002, 2, 849−851.

(25) Spichiger-Ulmann, M.; Augustynski, J. J. Appl. Phys. 1983, 54, 6061−6064.

(26) Cifuentes, S. C.; Monge, M. A.; Pérez, P. Corros. Sci. 2012, 57, 114−121.

(27) Van Rooij, G. J.; Veremiyenko, V. P.; Goedheer, W. J.; de Groot, B.; Kleyn, A. W.; Smeets, P. H. M.; Versloot, T. W.; Whyte, D. G.; Engeln, R.; Schram, D. C.; Lopes Cardozo, N. J. Appl. Phys. Lett. 2007, 90, 121501-1−121501-3.

(28) Krashenninikov, S. I. Phys. Scr. 2011, T145, 014040-1−014040-4.

(29) Al Mohammad, A.; Gillet, M. Thin Solid Films 2002, 408, 302−309.

(30) Granqvist, C. G. Sol. Energy Mater. Sol. Cells 2000, 60, 201−262.

(31) Sato, R.; Kawamura, N.; Tokumaru, H. Appl. Surf. Sci. 2008, 254, 7676−7678.

(32) Wriedt, H. A. Bull. Alloy Phase Diagrams 1989, 10, 368−384.

(33) Migas, D. B.; Shaposhnikov, V. L.; Rodin, V. N.; Borisenko, V. E. J. Appl. Phys. 2010, 108, 093713-1−093713-7.

(34) Sikka, V. K.; Rosa, C. J. Corros. Sci. 1980, 20, 1201−1219.

(35) Murphy, A. B. Sol. Energy Mater. Sol. Cells 2007, 91, 1326−1337.

(36) Lopez, R.; Gomez, R. J. Sol-Gel Sci. Technol. 2012, 61, 1−7.

(37) González-Borrero, P. P.; Sato, F.; Medina, A. N.; Baesso, M. L.; Bento, A. C.; Baldissera, G.; Persson, C.; Niklasson, G. A.; Granqvist, C. G.; Ferreira da Silva, A. Appl. Phys. Lett. 2010, 96, 061909-1−061909-3.

(38) Liu, X.; Wang, F.; Wang, Q. Phys. Chem. Chem. Phys. 2012, 14, 7894−7911.

(39) Ahn, K.-S.; Lee, S.-H.; Dillon, A. C.; Tracy, C. E.; Pitts, R. J. Appl. Phys. 2007, 101, 093524-1−093524-4.

(40) Mi, Q.; Zhanaidarova, A.; Brunschwig, B. S.; Gray, H. B.; Lewis, N. S. Energy Environ. Sci. 2012, 5, 5694−5700.

(41) Kajita, S.; Yoshida, N.; Yoshihara, R.; Ohno, N.; Yokochi, T.; Tokitani, M.; Takamura, S. J. Nucl. Mater. 2012, 421, 22−27.

(42) Yajimaa, M.; Hatanob, Y.; Kajitac, S.; Shib, J.; Harab, M.; Ohno, N. J. Nucl. Mater. 2013, 438, S1142−S1145.

(43) Bange, K. Sol. Energy Mater. Sol. Cells 1999, 58, 1−131.